Check for updates

# Recent progress in TiO₂–biochar-based photocatalysts for water contaminants treatment: strategies to improve photocatalytic performance

Yunfang Liu,[a] Xiaowei Dai,[b] Jia Li,[a] Shaoheng Cheng,[c] Jian Zhang[a] and Yibo Ma ⓘ *[a]

Toxic organic pollutants in wastewater have seriously damaged human health and ecosystems. Photocatalytic degradation is a potential and efficient tactic for wastewater treatment. Among the entire carbon family, biochar has been developed for the adsorption of pollutants due to its large specific surface area, porous skeleton structure, and abundant surface functional groups. Hence, combining adsorption and photocatalytic decomposition, TiO₂–biochar photocatalysts have received considerable attention and have been extensively studied. Owing to biochar's adsorption, more active sites and strong interactions between contaminants and photocatalysts can be achieved. The synergistic effect of biochar and TiO₂ nanomaterials substantially improves the photocatalytic capacity for pollutant degradation. TiO₂–biochar composites have numerous attractive properties and advantages, culminating in infinite applications. This review discusses the characteristics and preparation techniques of biochar, presents *in situ* and *ex situ* synthesis approaches of TiO₂–biochar nanocomposites, explains the benefits of TiO₂–biochar-based compounds for photocatalytic degradation, and emphasizes the strategies for enhancing the photocatalytic efficiency of TiO₂–biochar-based photocatalysts. Finally, the main difficulties and future advancements of TiO₂–biochar-based photocatalysis are highlighted. The review gives an exhaustive overview of recent progress in TiO₂–biochar-based photocatalysts for organic contaminants removal and is expected to encourage the development of robust TiO₂–biochar-based photocatalysts

[a]*School of Sciences, Beihua University, Jilin 132013, China. E-mail: yiboma@beihua.edu.cn*

[b]*Department of Reproductive Medicine Center, The Second Norman Bethune Hospital of Jilin University, Changchun, 130041, China*

[c]*State Key Laboratory of Superhard Materials, College of Physics, Jilin University, Changchun 130012, China*

*Yunfang Liu is a graduate student in the School of Science at Beihua University under the supervision of Dr Yibo Ma. Her research directions mainly focus on preparing TiO₂–biochar-based materials and their applications in photocatalysis.*

**Yunfang Liu**

*Dai Xiaowei, an attending physician, works at the Second Hospital of Jilin University in Changchun, China. He mainly studies urology and male reproductive diseases, such as male infertility, sexual dysfunction, and assisted reproductive technology. Academic Part-time: Young member of the Andrology Branch of the Chinese Society of Traditional Chinese Medicine Information. Young member of the Reproductive*

**Xiaowei Dai**

*Medicine Branch of Wu Jieping Foundation. Youth member of the Reproductive Medicine Branch of the Chinese Society of Traditional Chinese Medicine. Member of the Standing Committee of the Maternal and Child Health and Andrology Society of the Chinese Sexuality Society.*

for sewage remediation and other environmentally friendly uses.

## 1. Introduction

Global concern has been sparked by the fact that water pollution endangers human life and harms ecosystems.[1,2] It has been reported that numerous toxic organic contaminants, such as phenolic compounds, polymers, cyanides, and detergents, reside in sewage.[3–6] Several human diseases, even cancer, have been related to organic pollutants in water.[7,8] Therefore, hazardous contaminants found in wastewater must be appropriately disposed of to protect human health and the environment and to guarantee safe discharge. Most organic pollutants are recalcitrant, toxic, and have weak biodegradability. Thus, they cannot be degraded absolutely *via* traditional treatment techniques (for example, adsorption, biodegradation, and

direct burning).[9,10] Developing a promising treatment technology is paramount for effectively degrading contaminants and ensuring sustainable development. The photoelectrocatalytic water splitting experiment for $H_2$ evolution under ultraviolet light in 1972 led to the development of photocatalysis technology.[11,12] Notably, solar energy is a renewable, clean resource, and photocatalytic technology as an advanced oxidation process offers compelling advantages over conventional strategies for coping with chemical pollutants, such as mild reactions, no additional emissions, high degradation efficiency, and energy savings.[13–15]

The core of photocatalytic degradation of pollutants is to develop highly efficient and inexpensive photocatalysts. Titanium dioxide ($TiO_2$) nanoparticles are now regarded as one of the best photocatalytic materials because they have unique electrical and optical properties, are chemically stable, and don't harm living things.[16] However, the $TiO_2$ photocatalyst, which has a broad energy band gap (3.0–3.2 eV) and can only soak up radiation in the near ultraviolet (UV) zone (approximately 5% of the total sunlight spectrum), is limited to visible light applications.[17] Furthermore, most single-component photocatalysts are provided in the form of tiny particles (such as nanoscale), which effectively increases the specific surface area of the material and aids in enhancing the photocatalytic effect. However, it is more noteworthy that tiny particles can also greatly enhance the intermolecular force, leading to agglomeration effects during the treatment of pollutants, which hinder the effective decomposition of pollutants. At the same time, the recycling and reuse of nanoscale catalysts also face challenges.[18] To alleviate the drawbacks, integrating photocatalytic materials with substrate materials for modification has been gradually developed and utilized. Representative substrates, including carbon materials (like activated carbon, multiwalled carbon nanotube, and reduced graphene oxide),

*Jia Li received her B.S. in Physics from Changchun University in Jilin, China in 2010, and her M.S. and Ph.D. in condensed matter physics from Jilin University in China in 2015. She works at the School of Science at Beihua University in Jilin, China. For many years, she has been engaged in the research and development of new materials and physical properties. Her current research focuses on developing new carbon-based related materials, such as low-dimensional diamond and boron–carbon–nitrogen sandwich structures, exploring new structures and their electronic and optical properties, and expanding their applications in photocatalysis, nanoelectronic devices, and sensors.*

**Jia Li**

*Jian Zhang received his Ph.D. degree from Jilin University in 2016. He is now a Graduate Supervisor at the College of Science Beihua University. His research focuses on the synthesis and characterization of low-dimensional layered nanomaterials and the structural design and physical properties of nanomaterials under high pressure conditions.*

**Jian Zhang**

*Yibo Ma received his B.S. in Physics from Jilin Normal University, Siping, China, in 2012 and his M.S. and Ph.D. in condensed matter physics from Jilin University, Changchun, China, in 2017. He works at the School of Science at Beihua University in Jilin, China. He won the "Best Researcher Award" at the "International Research Awards on Advanced Nanomaterials and Nanotechnology" in 2023 for his pioneering contributions to nanomaterials design for the photocatalysis field. His current research focuses on preparing carbon-based materials such as biochar and diamond and their applications in photocatalysis, supercapacitors, and biosensors.*

**Yibo Ma**

zeolites, porous polymers, and metal–organic frameworks have been employed to investigate desirable, high-performance photocatalytic materials.[19–21] Considering the quick recombination rate of photoinduced carriers and the low thermal stability of most substrates, carbon materials are superior in photocatalytic degradation applications.[22] Carbon–$TiO_2$ composites have drawn growing interest as outstanding photocatalysts since carbon materials can serve as electron traps for gathering photoinduced carriers from the photocatalyst surface.[23,24] At the same time, carbon doping is an efficient approach for introducing impurities into the $TiO_2$ lattice, which decreases the band gap and extends visible light absorption.[25] Biochar is extraordinarily competitive among carbonaceous materials due to its rich in natural resources, non-metallic nature, acid and alkali resistance, and exceptional ecological sustainability, as well as its good physicochemical characteristics, including a high specific surface area, a porous framework, oxygen-containing groups, intrinsic minerals, and active binding sites.[26–28] These characteristics are advantageous for the binding and growth of photocatalyst nanoparticles, leading to significant loadings, robust stability, and remarkable organic waste photodegradation capabilities.[29,30] Therefore, biochar is an excellent support for $TiO_2$-based catalysts, and in recent years, $TiO_2$–biochar-based photocatalysts have been recommended and studied widely.

The combination of $TiO_2$ semiconductor and biochar offers several advantages:

(1) Pristine biochar is an appropriate photocatalytic material.[31–34] Several advanced oxidation processes, like Fenton-like oxidation, photocatalysis, sonocatalysis, and electrocatalysis, have utilized biochar catalysts.[35–38]

(2) As a supporting material for $TiO_2$ photocatalysts, biochar has a stable structure and easy recovery.

(3) The porous structure and large specific surface area of biochar provide solid guarantees for the adsorption of pollutants, which can effectively increase the contact between pollutants and $TiO_2$ photocatalysts, shorten the carrier migration path, and improve the photocatalytic effect.

(4) Biochar helps create vacancies, acting as photoelectron traps for captured $TiO_2$, thereby suppressing the annihilation of photogenerated $e^-–h^+$ pairs. Concurrently, biochar enhances the heat resistance of photocatalysts, reducing their band gap and boosting the response to light sources.[39]

(5) The composite, coupled with biochar and $TiO_2$ semiconductor, could present unique and complementary physicochemical properties in favor of water treatment applications.[40]

However, there are also many challenges associated with the combination of biochar and $TiO_2$ photocatalysts:

(1) The preparation method of the composite photocatalysts directly affects the bonding strength between biochar and $TiO_2$. The nonspecific binding of $TiO_2$ photocatalysts may lead to a significant decrease in their effectiveness over time.

(2) The impurities and functional groups in biomass, influenced by factors such as growth environment, can lead to unpredictable performance of each batch of prepared biochar.

(3) The strong biochar adsorption also hinders the recycling of composite photocatalysts.

(4) Improperly applied amounts of biochar shade the light of $TiO_2$ photocatalyst, affecting the generation efficiency of carriers.

It is time to review this intriguing topic to recapitulate current developments and, fundamentally, to acquire an in-depth knowledge of the application of $TiO_2$ biochar-based materials in photocatalytic decontamination. This review will concentrate on the synthesis methods, physicochemical properties, advantages, and photocatalytic capacity of $TiO_2$–biochar-based photocatalysts to remove organic effluent pollutants. Three aspects of some prospective photocatalytic efficiency enhancement strategies are highlighted. Lastly, the significant obstacles and prospects of photocatalysts based on $TiO_2$–biochar are presented.

## 2. Biomass for biochar production

Biochar is a unique and renewable carbonaceous substance derived from decomposing biomass residues in oxygen-depleted conditions.[41] Its porous structure and multitudinous oxygen-containing functional groups on its surface make it suitable for binding pollutant molecules.[42] In addition, biochar's fitting compatibility and catalytic properties make it an exceptional pollutant removal material for practical application in photocatalysis.[43]

### 2.1 Preparation methods of biochar

It is widely accepted that biomass is the primary source of biochar's feedstock. Carbon-rich biomasses can be regenerated from agricultural and forestry byproducts, garbage, woody products, plants, animal manures, and dietary leftovers.[44,45] It comprises both lignocellulosic (woody products, agricultural and forestry byproducts, plants) and non-lignocellulosic products (garbage and animal leftovers).[46,47] Thermochemical techniques can directly convert these numerous forms of biomass into biochar materials.[48] The most investigated thermochemical treatment methods are oxygen-limited pyrolysis and hydrothermal charring.

Pyrolysis is mainly divided into slow pyrolysis, fast pyrolysis, and flash pyrolysis. Among them, slow pyrolysis has been extensively adopted because of its substantial biochar yield, simple operation, and low cost.[49,50] Zhang et al.[51] produced biochar by pyrolyzing leftovers from a school cafeteria in oxygen-depleted conditions. The resultant biochar with an even surface was considered an appropriate supporter for attaching BiOBr. Zhang et al.[52] prepared biochar using crop straws as a precursor by pyrolysis at 600 °C for 120 min under limited oxygen conditions. Luo et al.[53] crushed poplar to obtain poplar sawdust and then heated it at 600 °C under $N_2$ atmosphere to obtain biochar (BC), which served as a conductive aisle in the $ZnFe_2O_4$/BC/ZnO composite to improve the transportation of photoexcited electrons. Meanwhile, pyrolysis could be used to fabricate biochar doped with other elements. For instance, Wang et al.[54] mixed urea and pine biochar at a particular mass ratio to produce N-modified biochar by pyrolyzing in a vacuum muffle furnace at 500 °C for 120 min. The heating temperature is one of the crucial points for producing biochar via pyrolysis.

According to previous studies,[55–57] researchers commonly set the heating temperature at 300–900 °C. Generally, the surface area and pore quantity of biochar increase as the degree of heat rises. However, pyrolyzing biomass at an excessively extreme temperature may cause the carbon skeleton to split, leading to the opposite result.[58,59] Various pyrolysis procedures will produce biochar with unique physicochemical features and varying application efficacy.[60] In addition, Shi et al.[61] prepared biochar with different pyrolysis temperatures, which manifested that the photocatalytic ability of biochar rose as pyrolysis temperature decreased. Therefore, an in-depth study of how heating temperature affects biochar's surface features and physicochemical characteristics is worthwhile for the further development of biochar. Overall, modulating heating rates and maintaining an exact response temperature could prove challenging in the pyrolysis process.[27]

The other efficient method for preparing biochar is hydrothermal carbonization (HTC). Typically, HTC is conducted at comparatively lower temperatures and more significant pressures for converting biomass to biochar.[62] Xu et al.[63] reported that N-doped carbons were generated by HTC at 200–260 °C using sewage sludge, rice husk, and cellulose as precursory biomass materials. Cai et al.[64] employed crushed peanut shells as raw biomass materials by hydrothermal reaction in the existence of iron chloride and hexamethylenediamine (HDA) to produce magnetic HDA-modified biochar. Liu et al.[65] added measured lotus powder to a nitrate solution ($La(NO_3)_3 \cdot 6H_2O$ and $Fe(NO_3)_3 \cdot 6H_2O$ were mixed with deionized water) and then carried out a hydrothermal reaction at 180 °C for 90 min. Lastly, C-doped $LaFeO_3$/biochar was produced by calcining the sample. Moreover, because carbon content relates directly to ash quantity and pyrolysis temperature, biochar with the desired carbon and ash content can be produced by modulating the hydrothermal temperature.[45] Compared with pyrolysis, HTC has a higher product yield (up to 88%) and lower energy consumption.[66] HTC is needed for subsequent processes, such as filtration, centrifugation, and drying, to obtain the desired biochar.

Besides that, the combination of pyrolysis and the HTC process has been conventionally utilized to dope elements into biochar or form biochar-based composites. Talukdar et al.[67] successfully synthesized $Ag_3PO_4$/$Fe_3O_4$ co-doped bamboo-derived activated biochar via two-step processes. Specifically, bamboo-derived activated biochar (BAB) was generated by pyrolysis at 500 °C, followed by a wet chemical process to produce an $Ag_3PO_4$/$Fe_3O_4$ co-doped BAB composite. Chen et al.[68] first prepared micro–mesoporous carbon sheets (MMCSs) by pyrolyzing the luffa sponge in a tubular furnace, followed by KOH activation. Then, the obtained MMCSs were mixed with thiourea and dispersed into the distilled water to construct micro–mesoporous carbon sheets doped with nitrogen and sulfur via a hydrothermal reaction.

Varying raw materials, production conditions, and modification techniques can alter the surface features of biochar.[49,69–71] The type of biomass material has the most significant impact on biochar's fixed carbon and ash contents. Biochar with a high ash content is unsuitable for capturing or eliminating contaminants due to its diminished adsorption sites and micropore surface areas.[49,72] Acid modification can remove the ash and organic matter from biochar, resulting in porous structures and oxygen-containing functional groups.[6,73–75] Biochar's specific surface area can be increased, and its aromaticity can be altered through alkali modification.[76] Besides, while metal modification might create additional catalytic active sites, pristine adsorption sites may be occupied, or porous structures may be blocked.[77] Thus, the design of the doping site and the loading ratio on biochar should be deeply considered. Overall, biochar's surface properties correlate with catalytic performance, so optimizing preparation strategies for biochar catalytic application is imperative.

## 2.2 Adsorption over pristine biochar

The remarkable characteristic of biochar is its adsorption capacity because of its porous nature, enormous specific surface area, and adequate functional groups.[78] Applications in the adsorption and decomposition of contaminants necessitate a porous material with a high surface area. The specific surface area and porosity may affect the biochar's adsorption capacity and the location of catalytically active sites, thereby determining its performance.[79] More opportunities for contaminants to connect with biochar surface functional groups and photocatalysts can be obtained in the biochar with a greater surface area and porosity, accelerating adsorption and decomposition rates. Composite photocatalysts are better at breaking down pollutants than single-phase materials because more pollutants stick to the surface of the composite, and more active species can be generated for degradation reactions.[26] To obtain porous and functionalized biochar, Ma et al.[80] mixed tobacco stem powder with $K_2CO_3$ and low-density polyethylene in a certain mass ratio, followed by pyrolyzing at 900 °C under Ar atmosphere. The produced biochar with an extensive specific surface area and porosity enhanced the potential for adsorption and promoted the separation of photogenerated carriers. In Wu et al.'s study,[81] potassium hydroxide-modified algae-based biochar was successfully fabricated by calcining in the muffle furnace. Briefly, 6 g of prepared biochar was combined with various proportions of KOH. Subsequently, the mixture was calcined in a muffle furnace at 800 °C. The prepared composite material (PEBC) with a weight ratio of 0.5 between biochar and KOH can achieve a maximum adsorption ability of 744.32 mg $g^{-1}$ for sulfamethoxazole, which is far superior to other adsorbents. The test results of PEBCs indicate that the introduction of KOH in the preparation process of macroalgal biochar can effectively modulate the pore structure of the material, increase specific surface area, expand pore volume, and optimize pore size distribution, ultimately obtaining more adsorption sites and promoting pore filling. It is worth noting that the K element in the raw material helps to generate reducing gases (CO and $H_2$) during the calcination process, which not only accelerates the formation of the biochar's porous structure but also reduces high-valence metals to low-valence states.[82]

The adsorption mechanism of biochar on pollutants varies at different pyrolysis temperatures, including multilayer

reaction, pore filling, mass transfer, π–π stacking interaction, and partition.[83,84] At low temperatures, electrostatic interactions and hydrogen bonding are the main factors; at high temperatures, the pore filling and π–π stacking interaction dominates.[31] Specifically, the oxygen-containing functional groups (hydroxyl, carboxyl, carbonyl, and ester groups) on the surface of biochar can rapidly adsorb pollutants and transfer them to photocatalysts through π–π stacking, electrostatic attraction, and hydrophobic interactions.[85] For example, Yu et al.[86] produced a ZnO/biochar composite photocatalyst that has strong electrostatic adsorption performance and can achieve a removal rate of 95.19% for MB.

## 3. Synthesis strategies for TiO$_2$–biochar-based photocatalysts

TiO$_2$ is commonly employed as a photocatalyst due to its various advantageous properties, such as effective oxidizing capability, extraordinary chemical stability, and low toxicity.[49,87,88] Biochar can be used as a supporting material and possesses excellent electrical conductivity, which has great applicability potential in the realm of photocatalytic oxidation.[11] Combining TiO$_2$ with biochar is required to enhance the photocatalytic efficiency of semiconductors to remove organic contaminants. Synthesis strategies for TiO$_2$–biochar-based materials have been widely investigated over the past few years. Generally, hydrothermal synthesis is a typical method to prepare TiO$_2$ nanoparticles. Regarding biochar, as mentioned above, a popular production process is biomass pyrolysis in oxygen-scarce environments.

Here, the preparation strategies of TiO$_2$–biochar-based nanocomposites will be introduced by two sectors: in situ approaches and ex situ synthesis strategies. TiO$_2$ growth and loading biochar onto TiO$_2$ can be achieved simultaneously using in situ synthesis approaches. Typically, in situ approaches include solvothermal synthesis, sol–gel, chemical co-precipitation, and pyrolysis. An ex situ manufacturing approach attains the biochar combination by reworking the produced TiO$_2$ and biochar. Ex situ strategies mainly include impregnation–calcination, microwave treatment, plasma treatment, hydrothermal process, and bio-chemical method. TiO$_2$–biochar-based photocatalysts synthesized in recent years using these methods are summarized in Table 1.

### 3.1 In situ synthesis

**3.1.1 Solvothermal synthesis.** The solvothermal method, analogous to hydrothermal, is widely applied to produce catalyst nanoparticles. The solvothermal reaction occurs by dissolving the poorly soluble or insoluble substances to generate crystals under relatively high temperatures and pressure in a closed system.[18] More importantly, the solvothermal method can yield well-crystalline nanomaterials by moderately tuning preparation conditions (such as temperature and residence time).[108] Biochar is introduced to TiO$_2$ precursor to fabricate TiO$_2$–biochar composites via the solvothermal method, an effective and typical in situ synthesis process. Using solvothermal, Wu et al.[103] successfully generated flower-like C, N co-doped, Ov-TiO$_2$/C composites. In detail, the prepared bagasse–urea complex was mixed into tetrabutyl titanate acetic

**Table 1** Summary of the preparation methods and their photocatalytic degradation activity of recently reported TiO$_2$–biochar-based photocatalysts

| Photocatalysts | Method | In/Ex situ | Pollutants | Maximum activity | References |
|---|---|---|---|---|---|
| PMBC@TiO$_2$ | Sol–gel | In situ | Sulfadiazine | 94.6% 150 min | 89 |
| TiO$_2$/pBC | Sol–gel | In situ | Sulfamethoxazole | 91.27% 180 min | 75 |
| TiO$_2$/biochar | Pyrolysis | In situ | Methyl orange | 96.88% 150 min | 90 |
| Pyrolytic char/TiO$_2$ | Sol–gel | In situ | Phenol | 99% 300 min | 91 |
| C–TiO$_2$ | Pyrolysis | In situ | Methylene blue | 59% 360 min | 92 |
| Biochar–TiO$_2$ | Chemical co-precipitation | In situ | Methylene blue | 99.2% 240 min | 93 |
| TiO$_2$–MCDs | Microwave treatment | Ex situ | Methylene blue | 83% 120 min | 94 |
| Biochar–nano TiO$_2$ | Sol–gel | In situ | Toluene | 70.1% 300 min | 82 |
| Ni-T/AC | Sol–gel | In situ | Crystal violet | 99% 120 min | 95 |
| C–TiO$_2$ | Microwave treatment | Ex situ | Tetracycline hydrochloride | 70% 120 min | 96 |
| TiO$_2$/Salvinia molesta | Impregnation–calcination | Ex situ | Acid orange 7 dye | 90% 240 min | 97 |
| TiO$_2$/D500 | Impregnation–calcination | Ex situ | Phenol | 77.7% 180 min | 11 |
| TiO$_2$@BC | Impregnation–calcination | Ex situ | Phenanthrene | 63.68% 180 min | 6 |
| C/TiO$_2$ | Plasma treatment | Ex situ | Formaldehyde | 73.7% 180 min | 98 |
| N–TiO$_2$/N–biochar | Pyrolysis | In situ | Methyl orange | 97.6% 90 min | 99 |
| Biochar–TiO$_2$ | Impregnation–calcination | Ex situ | Methyl orange | 97.1% 60 min | 100 |
| Zn–TiO$_2$/pBC | Sol–gel | In situ | Sulfamethoxazole | 81.21% 180 min | 73 |
| Ag-doped biochar/g-C$_3$N$_4$/TiO$_2$ | Solvothermal synthesis | In situ | TC-HCl | 90.4% 80 min | 26 |
| TiO$_2$/BC | Sol–gel | In situ | Reactive Brilliant Blue KN-R | 99.71% 60 min | 101 |
| TiO$_2$/Fe–C | Solvothermal synthesis | In situ | Acetaminophen | 100% 360 min | 102 |
| Ag/C, N co-doped, Ov-TiO$_2$/C | Solvothermal synthesis | In situ | 2,4-Dichlorophenol | 95% 150 min | 103 |
| Biochar/TiO$_2$ | Sol–gel | In situ | Sulfamethoxazole | 91% 360 min | 104 |
| Ag/TiO$_2$/biochar | Pyrolysis | In situ | Methyl orange | 97.48% 60 min | 105 |
| N–TiO$_2$–Fe$_3$O$_4$–biochar | Pyrolysis | In situ | Methylene blue | 99.99% 300 min | 106 |
| Biochar–TiO$_2$ | Impregnation–calcination | Ex situ | Diclofenac | 90% 120 min | 107 |
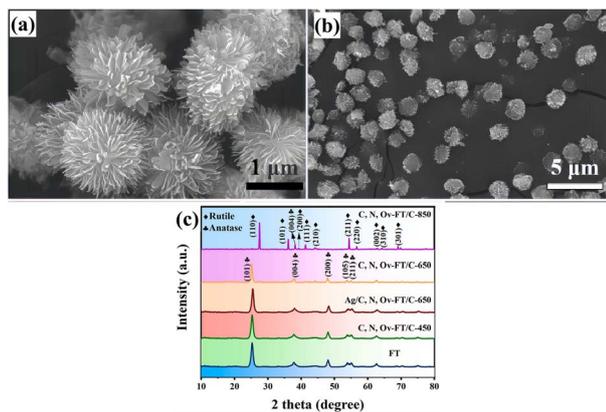
Fig. 1 (a) SEM images of flower-like TiO$_2$, (b) C, N, Ov-flower-like TiO$_2$/C-650. (c) Typical XRD patterns of as-prepared all samples.[103]

acid solution, and then the mixed solution initiated a solvothermal reaction in an autoclave at 180 °C for 720 min. The final product was sintered at 450 °C in N$_2$ atmosphere for 120 min. Fig. 1(a) and (b) is the SEM of the obtained samples. The characterization result showed that the flower-like TiO$_2$ particles were successfully decorated on the surface of biochar. In Fig. 1(c), the XRD pattern indicated that as-prepared flower-like TiO$_2$ particles show a classical anatase structure and a few weak peaks of the rutile phase. Therefore, the solvothermal method is efficient and convenient for preparing TiO$_2$–biochar nanocomposites.

**3.1.2 Sol–gel.** Sol–gel refers to the method by which organic metal compounds or inorganic salts are solidified through solution, sol, gel, and heat-treated to become oxides or other solid compounds.[9] For example, synthesizing of TiO$_2$–biochar nanocomposites, the biochar and titanate are stirred evenly in a specific solvent. Then, the pH of the solution is adjusted by nitric acid, and finally, the anti-solvent is added to form a sol. At the same time, the sample can be heated to accelerate the gelation process.[109] Fig. 2 is the flow chart of Guo et al.[82] preparing biochar–nano TiO$_2$ cross-linked structure by sol–gel method. He first added rice husk biochar to anhydrous ethanol containing tetrabutyl titanate and diluted nitric acid, then calcined the dried sample at 400 °C under N$_2$ protection. The heat treatment process can remove the organic compounds and accelerate the crystallization of sol–gel oxides.[110] The specific surface area of biochar–nano TiO$_2$ is 779.87 m$^2$ g$^{-1}$, which is 6.5 times that of pure TiO$_2$. This also directly proves that the
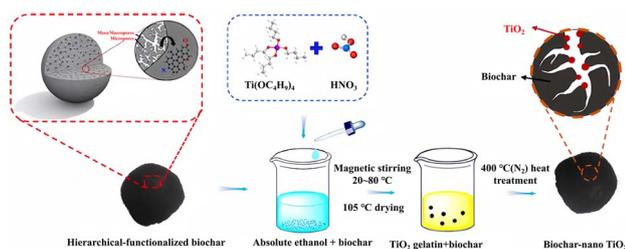
composite of biochar and TiO$_2$ can effectively increase the specific surface area of the sample and further enhance the adsorption performance of the material for pollutants in the photocatalytic process.

**3.1.3 Chemical co-precipitation.** Chemical co-precipitation is an essential and straightforward strategy for synthesizing metal oxide catalysts, which is performed by combining anions and cations in a solution and producing insoluble solid precipitation.[9] Fazal et al.[93] synthesized biochar–TiO$_2$ composites using a wet precipitation approach. In brief, already prepared biochar (produced from macroalgae by pyrolysis) was dispersed in isopropanol, followed by the dropwise addition of titanium(IV) isopropoxide. The product was then elevated to 80 °C to exhaust the solvent. The sample was then placed in a muffle furnace heated to 400 °C with airflow for 300 min. The SEM images exhibited that the spherical TiO$_2$ nanoparticles were evenly modified onto the biochar surface. Also, Herath et al.[111] successfully decorated Fe$_2$TiO$_5$ nanoparticles on biochar (BC) using a chemical co-precipitation method and a heat treatment process. The XRD examination of Fe$_2$TiO$_5$ and Fe$_2$TiO$_5$/BC corroborated the successful deposition of Fe$_2$TiO$_5$ on the biochar surface.

**3.1.4 Pyrolysis.** Mian et al.[106] fabricated N-doping TiO$_2$–Fe$_3$O$_4$–biochar composites through one-step pyrolysis of FeCl$_3$–Ti(OBu)$_4$ laden agar biomass, and the formation of N-doping was achieved via under NH$_3$ atmosphere. TiO$_2$ obtained by hydrolyzing tetrabutyl titanate is in situ grown onto biochar, followed by pyrolysis, a feasible synthetic path of TiO$_2$–biochar composites. Luo et al.[112] added tetrabutyl titanate into distilled water solution and introduced as-prepared biochar into the system. The solution was vigorously stirred to ensure that biochar was well distributed. Subsequently, the obtained dried TiO$_2$/biochar intermediates were activated at 500 °C for 120 min to form TiO$_2$/biochar composites.

### 3.2 Ex situ synthesis

**3.2.1 Impregnation–calcination.** Recently, Li et al.[6] effectively utilized the soaking calcination to synthesize TiO$_2$@BC ex situ, which differs from the in situ chemical co-precipitation method, where the already prepared TiO$_2$ was directly used. In addition, it can be adopted that TiO$_2$ and biochar are mixed by manual mechanical grinding, followed by calcining to prepare the composites. For instance, Lazarotto et al.[107] pyrolyzed the mixture of spent coffee biomass and TiO$_2$ via manual mechanical mixing to prepare biochar–TiO$_2$ composites. In the procedure, the biomass was converted into TiO$_2$-impregnated biochar. Therefore, employing the impregnation–calcination method to prepare TiO$_2$–biochar-based photocatalysts is attractive owing to its easy operation, cost-effectiveness, and reduced refuse production.

**3.2.2 Microwave treatment.** Microwave treatment is an advanced technology for the ex situ synthesis of TiO$_2$–biochar-based photocatalysts. Its prominent advantages are short heating treatment time and a safe operation process. The microalgae-based carbon dots (MCDs) were adorned on the outside of TiO$_2$ nanoparticles by Vu Nu et al.[94] via



Fig. 2 Preparation process of biochar–nano TiO$_2$.[82]

a straightforward microwave procedure. Due to the incorporation of MCDs, the photodegradation efficiency of the $TiO_2$–MCDs composite was enhanced. In particular, as photosensitizers of electron acceptors, MCDs can acquire photogenerated electrons and boost the utilization of visible light. Notably, microwave power exerts a significant influence on the properties of synthesized composites.[49] Oseghe and his coworker[96] fabricated pine cone-derived C-doped $TiO_2$ composites by microwave heating treatment at 600, 800, and 1000 W powers (labeled CT600, CT800, and CT1000, respectively). The studies showed that the BET surface area of composites decreased as microwave power increased. CT800 is better at breaking down tetracycline hydrochloride than other composites because it is more catalytic, has a lower rate of photogenerated carrier annihilation, and has more active species for the redox reaction.

**3.2.3 Plasma treatment.** Dielectric barrier discharge (DBD), a promising technique for preparing and modifying photocatalysts, has been shown to broaden the utilization of $TiO_2$ in the non-UV region.[113] Several reports have demonstrated that titanium undergoes a transformation of its crystalline and amorphous crystal structures after hydrogen plasma etching, which can promote the utilization of visible light, reduce the binding of photoinduced carriers, and facilitate elemental doping, thus having an extended application in environmental protection.[114] Recently, Tan et al.[98] successfully synthesized bamboo carbon/$TiO_2$ composites by $H_2$ plasma using the DBD method (Fig. 3). The results showed that the composite with a 5% bamboo carbon weight ratio has a more meso/microporous structure, narrower band gap width, and lower electron–hole complexation rate and exhibits a good removal effect on formaldehyde.

**3.2.4 Other methods.** Some new protocols for preparing $TiO_2$–biochar-based photocatalysts, such as the hydrothermal process and bio-chemical method, have been developed for *ex situ* synthesis. Recently, Alomairy et al.[32] adopted the bio-chemical method for synthesizing biochar-modified $TiO_2$/$CoFe_2O_4$ core–shells. The primary process of integrating biochar with the $TiO_2$/$CoFe_2O_4$ core–shell is ultrasonic irradiation, which is considered a feasible and effective tactic. Characteristic results displayed that biochar is conducive to reducing the



**Fig. 3** Sketch of the hydrogen dielectric barrier discharge modified system.[98]

agglomeration of $TiO_2$/$CoFe_2O_4$ core–shell nanoparticles. Sánchez-Silva et al.[115] prepared hydrochar–$TiO_2$ composite (HC–$TiO_2$) *via* a hydrothermal process using *Byrsonima crassifolia* stones (BCS) as biomass materials. Photodegradation experiments showed that HC–$TiO_2$ can achieve 77% removal efficiency of crystal violet ($20 mg L^{-1}$) within 90 min under UV light. Also, the reusability experiments indicated that the HC–$TiO_2$ composite has excellent stability for 5 times cycles.

# 4. Advantages of $TiO_2$–biochar-based materials in photocatalytic degradation

We summarized some of the latest $TiO_2$–biochar-based photocatalysts and $TiO_2$–non-biochar-based photocatalysts in Table 2. The results indicated that $TiO_2$–biochar-based photocatalysts generally exhibited superior photocatalytic performances and larger specific surface areas than $TiO_2$–non-biochar-based photocatalysts. In detail, the advantages of $TiO_2$–biochar-based materials in photocatalytic degradation can be embodied in five aspects as follows:

## 4.1 Abundant reserves

Biomass contains nearly all of the living things on the planet and the biological material produced, processed, and expelled by them.[116] Its broad existence and plentiful stocks ensure the creation of $TiO_2$–biochar composites. Therefore, biochar has a conspicuous advantage in feedstock costs compared to other carbon materials and serves an essential function green energy. Moreover, $TiO_2$ nanomaterials that are cost-effective and have low toxicity can achieve a promising and long-term application in photocatalysis. Consequently, from the perspective of reserves, $TiO_2$–biochar materials are recommended for cheap manufacturing and a green economy.

## 4.2 Large specific surface area

$TiO_2$–biochar-based nanocomposites derived from biomass materials as carbon sources possess large specific surface areas because of biomass carbon's natural hierarchical porous microstructure.[117] Specifically, macropores promote rapid fluid movement, whereas mesopores and micropores ensure complete interaction between contaminants and the photocatalyst surface. Also, biochar with a more porous structure makes $TiO_2$–biochar-based photocatalysts better at capturing light by taking advantage of how light reflects and scatters in the pores. More importantly, the surface active centers and exposed atoms of the materials increase with specific surface areas. These active sites and unsaturated atoms help stabilize the catalytic process's intermediates and reduce the activation barrier.[118] In our previous study,[34] we reported a novel Au nanoparticles/$TiO_2$ nanorods/biochar (Au/$TiO_2$/BCP) photocatalyst with a massive specific surface area of $1291.10 m^2 g^{-1}$. Photodegradation results demonstrated that Au/$TiO_2$/BCP reached a removal efficiency of 98.4% for degradation tetracycline, and per unit mass can remove 492 mg tetracycline.
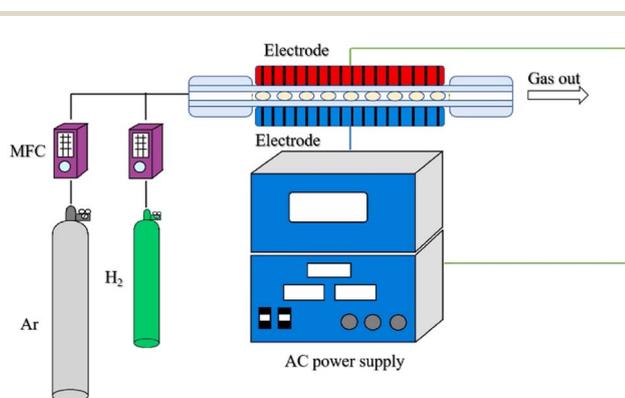
**Table 2** Comparisons of the photocatalytic properties of $TiO_2$–biochar-based photocatalysts and $TiO_2$–non-biochar–based photocatalysts

| Photocatalysts | Biochar-based/non-biochar based | Light source | Pollutants | Dosage (mg) | Efficiency | $S_{BET}$ (m² g⁻¹) | $M^a$ (mg g⁻¹) | References |
|---|---|---|---|---|---|---|---|---|
| Au/TiO₂/BCP | Biochar-based | 400 W mercury lamp | Tetracycline 40 mg L⁻¹ (100 mL) | 8 | 98.4% (180 min) | 1291.1 | 492 | 34 |
| AC/TiO₂ | Biochar-based | UV light | 17α-Ethinylestradiol 6 mg L⁻¹ (10 mL) | 5 | 96.23% (120 min) | 34.28 | 11.5 | 125 |
| TiO₂/BC | Biochar-based | 30 W UV lamp | Bisphenol A 50 mg L⁻¹ (100 mL) | 100 | 97.6% (60 min) | 821 | 48.8 | 126 |
| BC/A/R-TiO₂ | Biochar-based | 300 W xenon lamp | Tetracycline 50 mg L⁻¹ (250 mL) | 100 | 99.5% (120 min) | 315.8 | 124.4 | 127 |
| TiO₂/CNTs | Non-biochar-based | 1000 W xenon lamp | Methylene blue 30 mg L⁻¹ (100 mL) | 200 | 86.95% (180 min) | — | 13 | 128 |
| TiO₂-graphene | Non-biochar-based | 250 W mercury lamp | Phenol 10 mg L⁻¹ (300 mL) | 300 | 89.56% (240 min) | 62.728 | 8.9 | 129 |
| N-doped TiO₂/SiO₂ | Non-biochar-based | 16 W LED light | Methylene blue $1 \times 10^{-5}$ M (100 mL) | 100 | 72% (720 min) | 115.4 | — | 130 |
| TiO₂/MXene | Non-biochar-based | 500 W mercury lamp | Methylene blue 60 mg L⁻¹ (20 mL) | 10 | 96.44% (60 min) | 60.47 | 115.7 | 131 |
| ZIF-67/F-TiO₂ | Non-biochar-based | 500 W xenon lamp | Tetracycline 20 mg L⁻¹ (100 mL) | 30 | 87% (60 min) | 73.93 | 58 | 132 |

$^a$ $M$ (mg g⁻¹) is denoted as the pollutant mass removed by per unit mass of photocatalyst.

Therefore, the pollutant degradation rate is considerably improved using $TiO_2$–biochar-based photocatalysts.

### 4.3 Boosting the adsorption of pollutants

Since the photocatalytic oxidation process happens on the exterior of the photocatalyst, a superior surface-based adsorption performance is necessary for the efficient destruction of contaminants.[119] Biochar has more surface functional groups (such as hydroxyl and carboxyl groups) than activated carbon, which is one of the most pivotal factors influencing adsorption efficacy.[120] As a result, more pollutants in wastewater can be adsorbed and decomposed near the surface of photocatalysts, thereby achieving high photocatalytic efficiency, which is a crucial step in developing feasible applications of photocatalysts in wastewater treatment.

### 4.4 Strong interaction between biochar and $TiO_2$

Owing to the strong interaction between carbon materials and metal Ti atoms, biochar and $TiO_2$ can form a close contact structure. This improves the material's physical and chemical properties and the separation and migration of photoinduced charge, enhancing the lifetime of carriers and making them less likely to recombine.[121] For instance, Zhai et al.[122] manifested that $TiO_2$/bio-char had higher abilities of adsorption and decomposition for methylene blue than the bio-char, for which this composite existed a benign interaction between $TiO_2$ and bio-char and offered an enhanced electron transport efficiency.

### 4.5 Accelerating charge migration in the $TiO_2$–biochar-based composites

In a $TiO_2$–biochar composite photocatalysis system, biochar with appropriate conductivity can serve as an electron trap and a transit channel, promoting the separation and migration of photoinduced charge carrier pairs of $TiO_2$ and boosting the redox reaction. Furthermore, more reactive oxygen species can be generated by $TiO_2$–biochar composites, thereby enhancing the photocatalytic activity.[123] Hsu et al.[124] successfully deposited $TiO_2$ on the carbon nanospheres to construct carbon@titania yolk–shell nanostructures. The XRD results (Fig. 4a) indicated that $TiO_2$ hollow nanospheres prepared by sol–gel and calcination possess anatase structure. As shown in Fig. 4b, owing to the presence of carbon nanospheres, photoexcited electrons on the $TiO_2$ can be transferred, effectively inhibiting the recombination of electron–hole pairs.
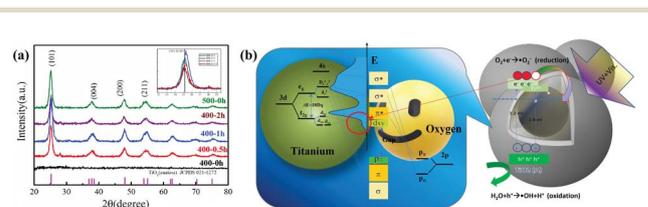


**Fig. 4** (a) X-ray diffraction patterns of nanospheres. (b) The mechanism of mobile electron transfer and hole increase under UV-vis illumination.[124]

# 5. Strategies for improving photocatalytic performance of TiO₂–biochar-based photocatalysts

## 5.1 In terms of biochar

The improved strategies for biochar can be concluded in two aspects. For one thing, the preparation temperature of biochar was found to have significant effects on its features and the performance of the $TiO_2$–biochar photocatalyst. Xie et al.[133] fabricated biochar utilizing three distinct pyrolysis temperatures (300–700 °C). The results demonstrated that the $TiO_2$–biochar prepared at 500 °C displayed the most effective purification of manufactured rainwater, as the stable tubular structure of the biochar facilitated $TiO_2$ nanoparticle attachment. For another, the surface modification of biochar is a vital point in achieving a uniform dispersion of nano-$TiO_2$ photocatalysts. Acid oxidization can erode the biochar surface, introduce functional groups, and expose more adsorption sites conducive to controllable superficial growth.[104,134] The $TiO_2$ particles loaded on the surface of acid-treated biochar are smaller than those on untreated surfaces. This is because acid oxidation can effectively reduce the clumping of nanoparticles.[82] Besides, biochar with a hierarchical porous structure can be achieved via activating an alkali, such as KOH.[101,135] As a result, selecting suitable preparation conditions and functionalized treatment technology for biochar is an attractive tactic for enhancing its physical and chemical characteristics.

## 5.2 In terms of TiO₂

The exposed facets of nanocrystals can easily affect chemical reactions on the external layers of photocatalysts during the photodegradation process. More importantly, different crystal facets present different surface atomic arrangements and crystallographic orientations, which determine the spatial charge separation between facets and reactive sites and diverse molecule absorption abilities.[136,137] Qu et al.[138] investigated the photocatalytic water splitting performance of anatase $TiO_2$ with predominant {001} facets and {111} facets, showing that the {001} facets displayed higher activity. The substantial amount of surface undercoordinated Ti atoms and the surface atoms' strained configuration are advantageous for water adsorption and dissociation. Besides, as shown in Fig. 5, in situ photochemical probing reactions have corroborated that more nucleation sites exist on the {001} facets of anatase $TiO_2$. In addition, utilizing the strong oxidation ability of $TiO_2$ (001) facets, Li et al.[139] successfully designed a $MoS_2$/Au/$TiO_2$ heterogeneous photocatalyst with highly-exposed (001) facets of $TiO_2$. Notably, the photogenerated holes in this composite are primarily on the large $TiO_2$ (001) facets. This means that more oxidation sites are exposed, which speeds up the photocatalytic removal process. Thus, to boost the photocatalytic capacity of $TiO_2$–biochar-based photocatalysts, it is crucial to tune the exposed facets of $TiO_2$ nanocrystals during the manufacture of $TiO_2$–biochar-based composites.

On the other hand, controlling the configuration of $TiO_2$ nanocrystals at the microscopic level cannot merely accelerate the movement of charges but also facilitate mass delivery, resulting in an enhanced photocatalytic performance for the disintegration of organic toxins.[140] Herein, Song et al.[141] synthesized $TiO_2$ nanomaterials with three different morphologies (nanocones, nanorods, and nanoparticles) using a $Na_2$-EDTA-assisted hydrothermal technique (Fig. 6a), which were used as catalysts for the photoelectrocatalytic (PEC) removal of pollutants. The outcomes of the degradation experiment revealed that the nanocone-shaped $TiO_2$ (99.3%) had superior PEC performance compared to the nanorod-shaped $TiO_2$ (82.8%) and nanoparticle-shaped $TiO_2$ (62.7%) (Fig. 6b). This makes it easier to complete the mass transfer between catalysts with a conical array structure. Notably, the nanocone structure possesses a potent built-in electric field that facilitates carrier separation and migration, a prerequisite for producing active oxides. In addition, Zhang et al.[142] synthesized well-aligned sub-10 nm $TiO_2$ nanowire arrays with adjustable corrugated structures by a distinctive mono micelle-directed assembly tactic (Fig. 7). Characterization results demonstrated that ultrathin corrugated $TiO_2$ nanowire arrays could separate photocarriers, transfer charges, and activate surface holes all at the same time.
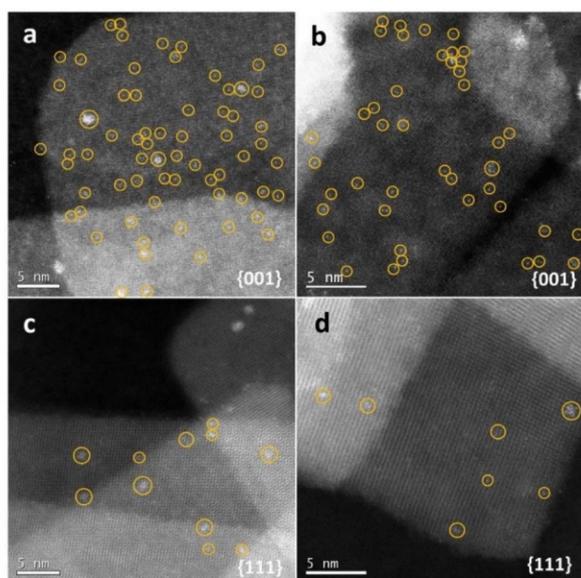


Fig. 5 Photo-deposition of Pt on different facets after one minute of illumination. (a and b) HAADF images of Pt deposited on {001} facets. (c and d) HAADF images of Pt deposited on {111} facets.[138]
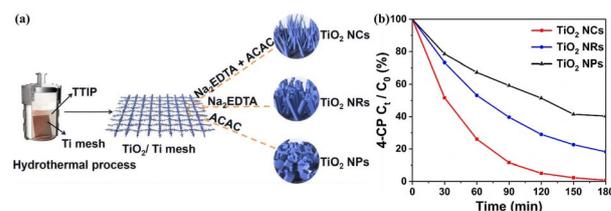


Fig. 6 (a) Synthesis scheme of $TiO_2$ catalysts with different structures by a $Na_2$EDTA-assisted hydrothermal approach. (b) The percentage of 4-CP degradation.[141]
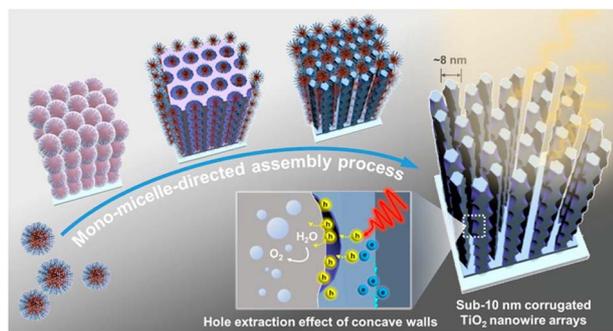
**Fig. 7** Schematic illustration of the formation process for the ultrathin corrugated $TiO_2$ nanowire arrays synthesized *via* the monomicelle-directed assembly approach.[142]

The remarkable optoelectronic behaviors are predominately determined by the exceedingly large surface area and rapid charge separation capability of the as-prepared, unusual $TiO_2$ arrangements. Consequently, it is desirable to finely manipulate the configuration of $TiO_2$ nanocrystals to ameliorate the photocatalytic efficiency of $TiO_2$–biochar-based photocatalysts.

### 5.3 The synergistic effect of biochar and $TiO_2$

Finding the optimal amount of carbonaceous material to add to $TiO_2$ when making $TiO_2$–biochar-based photocatalysts is important for biochar and $TiO_2$ to work together and for the photocatalytic activity to improve. Xie *et al.*[133] fabricated $TiO_2$–biochar composites using three various $TiO_2$–biochar mass proportion values by combining the necessary quantities of $TiO_2$ and biochar. The research results indicated that the purification effect of the $TiO_2$/biochar composite on artificial wastewater decreases with a decrease in mass ratio. This is because low mass ratio biochar blocks $TiO_2$, weakens the transmission between light and $TiO_2$, and loses photocatalytic efficiency.[143] However, too high a quality ratio can backfire, and the advantages of biochar materials cannot be fully utilized. Lu *et al.*[90] made several kinds of $TiO_2$/biochar composite catalysts with varying biochar-to-Ti mass ratios. They designated it as CT$x$, where $x$ ($x$ = 0.1/1, 0.2/1, 0.5/1, 0.8/1, 1/1) indicated the biochar-to-Ti mass ratios. In the photocatalytic oxidation experiments of methyl orange, CT0.2/1 showed the best effect, with a decolorization rate of nearly 97% and a mineralization rate of nearly 83%. It indicates a synergistic effect between biochar and catalyst, and adding a proper amount of biochar can promote the photocatalytic process.

Besides that, $TiO_2$–biochar nanocomposites with controllable porous microstructure and uniform morphology can be constructed *via* coupling with the template method, which contributes to the exposure of adequate activity sites for photocatalytic reactions. Wang *et al.*[144] fabricated hierarchical porous titanium dioxide/carbon nanocomposites ($TiO_2$/C) by introducing ice and nanoscaled silica as soft and hard templates for porosity modulating. The as-prepared $TiO_2$/C nanocomposites exhibited more effective photocatalytic activity compared to their counterparts lacking templating, which can be assigned to the instructed porous structure and distinctive

shape, which offer transfer avenues for electrolytes and photo-generated charge carriers, thereby enhancing the effectiveness of the degradation process.

## 6. Conclusions and future perspectives

In summary, $TiO_2$, as an excellent photocatalyst, has been applied for almost half a century. To overcome the drawbacks of $TiO_2$ and further broaden its application range, biochar, a novel carbonaceous material with fascinating physicochemical properties and environmental benignancy, is employed to couple with $TiO_2$ in the field of photocatalysis. Mainly, $TiO_2$–biochar-based composites have been extensively used to photodegrade organic contaminants in wastewater. Outstanding photocatalytic performance is required for $TiO_2$–biochar-based composites to be extensively applied and developed quickly. The reasoned design and manufacturing of $TiO_2$–biochar-based photocatalysts provide a potent means of enhancing the efficiency of light capture and photogenerated carrier separation. Through substantial research, multiple techniques and strategies have been adopted to prepare and modify $TiO_2$–biochar-based photocatalysts. In this review, we introduced the characteristics of biochar and summarized the synthesis approaches (including *in situ* and *ex situ* means), advantages, and strategies for optimizing the performance of $TiO_2$–biochar-based photocatalysts. However, $TiO_2$–biochar-based photocatalysts still need to be adequately explored. Although the distinctive advantages of $TiO_2$–biochar composites should be approved, the properties of $TiO_2$–biochar composites should be adequately researched, and the shortcomings of $TiO_2$–biochar-based photocatalysts in the application of photodegradation pollutants should be rationally realized. These preliminary investigations are essential for the advancement of photocatalysts based on $TiO_2$–biochar. In the following aspects, several significant improvements in the research on $TiO_2$–biochar-based photocatalysts can be accomplished.

First, as a dominating feature of biochar materials, the porous structure closely correlates with biochar's adsorption ability and photocatalytic performance. Meanwhile, the definite effect mechanisms have yet to be entirely explored. Thus, follow-up research concerning the mechanism of the porous structure of biochar remains to be done.

Second, regarding the combination of biochar and $TiO_2$ nanoparticles, the different loading proportions of $TiO_2$ on the surface and porous channels of biochar affecting photocatalytic activity have been extensively studied. Nonetheless, the specific interaction of $TiO_2$ load proportions and the as-synthesized composites of physical and chemical properties needs to be more explicit. In the future, the quantitative structure–activity relationship (QSAR) of $TiO_2$ load proportions and structural/optical features (*e.g.*, BET, pore volume, pore type, and light absorption ability) of $TiO_2$–biochar-based composites is desirable to investigate thoroughly, which has a significant effect on the understanding and reasonable design of high-performance $TiO_2$–biochar-based photocatalysts.

Third, the computational calculation for the pathways of TiO$_2$–biochar-based photocatalysts degradation pollutants is an effective means to investigate the decomposition process of pollutants. Unfortunately, limited by the fact that it is challenging to build the theoretical calculation model due to the complex structure of biochar, the theoretical calculation of photocatalytic degradation pollutants by TiO$_2$–biochar-based photocatalysts has yet to be developed comprehensively. More efforts on the theoretical calculation of TiO$_2$–biochar-based photocatalysts are necessary, including the adsorption mechanism between photocatalysts and pollutants, electrons transfer routes, and the minute decomposition pathway of contaminants.

Fourth, although we summarized many different methods for preparing TiO$_2$–biochar-based photocatalysts in this review, large-scale manufacture still needs to be improved in real-world applications. Also, the high production costs always limit the industrialization process of TiO$_2$–biochar-based photocatalysts. In order to decrease the costs of photocatalytic elimination of organic pollutants in water further using TiO$_2$–biochar-based photocatalysts, some appropriate strategies should be extensively investigated.

Fifth, most studies of TiO$_2$–biochar-based photocatalysts for the degradation of pollutants were implemented under UV light, although a favorable removal efficiency can be reached. Engineering strategies of TiO$_2$–biochar-based photocatalysts should be explored to tune intrinsic physicochemical properties and to expand the response of visible light. Besides, developing multi-functional and highly active TiO$_2$–biochar-based photocatalysts is needed to degrade the wastewater that consists of various persistent pollutants. Therefore, further investigation of TiO$_2$–biochar-based photocatalysts can focus on adjusting properties and regeneration to adapt to practical applications.

It is worth exploring these aspects we discussed, for which TiO$_2$–biochar-based materials have a promising future for photocatalytic degradation. Reasonable design and superior performance for TiO$_2$–biochar-based photocatalysts can conspicuously boost the development of wastewater treatment and energy conversion. This review will present a comprehensive cognizance of TiO$_2$–biochar-based photocatalysts. In the future, broader application fields of TiO$_2$–biochar-based materials could be realized through more research, such as applying them in solar cells, adsorption, and supercapacitors.

## Author contributions

YL: investigation, review, editing, writing—original draft; XD: review and editing; JL: review and editing; SC: investigation; JZ: review and editing; YM: investigation, writing, review, editing, validation, and supervision; all authors read and approved the final manuscript.

## Conflicts of interest

There are no conflicts to declare.

## Acknowledgements

## References

1 G. D. Değermenci, N. Değermenci, V. Ayvaoğlu, E. Durmaz, D. Çakır and E. Akan, *J. Cleaner Prod.*, 2019, **225**, 1220–1229.

2 J. Bai, R. Wang, Y. Li, Y. Tang, Q. Zeng, L. Xia, X. Li, J. Li, C. Li and B. Zhou, *J. Hazard. Mater.*, 2016, **311**, 51–62.

3 G. Rangarajan, A. Jayaseelan and R. Farnood, *J. Cleaner Prod.*, 2022, **346**, 131155.

4 M. Qiu, L. Liu, Q. Ling, Y. Cai, S. Yu, S. Wang, D. Fu, B. Hu and X. Wang, *Biochar*, 2022, **4**, 19.

5 C. N. C. Hitam and A. A. Jalil, *J. Environ. Manage.*, 2020, **258**, 110050.

6 J. J. Liu, S. N. Sun, J. Liu, Y. Kuang, J. W. Shi, L. Z. Dong, N. Li, J. N. Lu, J. M. Lin, S. L. Li and Y. Q. Lan, *J. Am. Chem. Soc.*, 2023, **145**, 6112–6122.

7 Q. Aemig, A. Helias and D. Patureau, *Water Res.*, 2021, **188**, 116524.

8 S. Wang and J. Wang, *Chem. Eng. J.*, 2019, **356**, 350–358.

9 R. B. Rajput, S. N. Jamble and R. B. Kale, *J. Environ. Manage.*, 2022, **307**, 114533.

10 Z. Guo, D. Kodikara, L. S. Albi, Y. Hatano, G. Chen, C. Yoshimura and J. Wang, *Water Res.*, 2023, **231**, 118236.

11 N. Hou, X. Li, X. Jiang, N. Zhang, R. Wang and D. Li, *Sci. Total Environ.*, 2022, **844**, 157145.

12 A. Fujishima and K. Honda, *Nature*, 1972, **238**, 37–38.

13 F. Li, T. Huang, F. Sun, L. Chen, P. Li, F. Shao, X. Yang and W. Liu, *Appl. Catal., B*, 2022, **317**, 121725.

14 M. Chen, Z. Ye, L. Wei, J. Yuan and L. Xiao, *J. Am. Chem. Soc.*, 2022, **144**, 12842–12849.

15 Y. Ma, X. Xu, T. Yang, Y. Shen, F. Jiang, Y. Zhang, X. Lv, Y. Liu, B. Feng, G. Che and L. Wang, *J. Alloys Compd.*, 2024, **970**, 172663.

16 S. Lotfi, K. Fischer, A. Schulze and A. I. Schafer, *Nat. Nanotechnol.*, 2022, **17**, 417–423.

17 S. Livraghi, M. C. Paganini, E. Giamello, A. Selloni, C. D. Valentin and G. Pacchioni, *J. Am. Chem. Soc.*, 2006, **128**, 15666–15671.

18 X. Liu, C. Wan, X. Li, S. Wei, L. Zhang, W. Tian, K.-T. Yong, Y. Wu and J. Li, *Front. Environ. Sci. Eng.*, 2020, **15**, 54.

19 S. Dekkouche, S. Morales-Torres, A. R. Ribeiro, J. L. Faria, C. Fontàs, O. Kebiche-Senhadji and A. M. T. Silva, *Chem. Eng. J.*, 2022, **427**, 131476.

20 H. Wang, X. Li, Y. Jiang, M. Li, Q. Xiao, T. Zhao, S. Yang, C. Qi, P. Qiu, J. Yang, Z. Jiang and W. Luo, *Angew Chem. Int. Ed. Engl.*, 2022, **61**, e202200465.

21 Y. Sun, G. Li, Y. Gong, Z. Sun, H. Yao and X. Zhou, *J. Hazard. Mater.*, 2021, **403**, 124019.

22 C. Sushma and S. G. Kumar, *Inorg. Chem. Front.*, 2017, **4**, 1250–1267.

23 M. M. Kandy, *Sustainable Energy Fuels*, 2020, **4**, 469–484.

24 A. Kongkanand and P. V. Kamat, *ACS Nano*, 2007, **1**, 13–21.

25 S. Yu, H. J. Yun, Y. H. Kim and J. Yi, *Appl. Catal., B*, 2014, **144**, 893–899.

26 J. Kuan, H. Zhang, H. Gu, Y. Zhang, H. Wu and N. Mao, *Nanotechnology*, 2022, **33**, 345402.

27 S. Ahmad, L. Liu, S. Zhang and J. Tang, *J. Hazard. Mater.*, 2023, **446**, 130727.

28 R. Shan, J. Han, J. Gu, H. Yuan, B. Luo and Y. Chen, *Resour., Conserv. Recycl.*, 2020, **162**, 105036.

29 Y. Luo, Y. Wang, F. Hua, M. Xue, X. Xie, Y. Xie, S. Yu, L. Zhang, Z. Yin, C. Xie and Z. Hong, *J. Hazard. Mater.*, 2023, **443**, 130300.

30 L. Shi, L. Liang, J. Ma, Y. Meng, S. Zhong, F. Wang and J. Sun, *Ceram. Int.*, 2014, **40**, 3495–3502.

31 T. Jiang, B. Wang, B. Gao, N. Cheng, Q. Feng, M. Chen and S. Wang, *J. Hazard. Mater.*, 2023, **442**, 130075.

32 S. Alomairy, L. Gnanasekaran, S. Rajendran and W. F. Alsanie, *Environ. Res.*, 2023, **238**, 117169.

33 J. Wang, G. Wang, T. Yu, N. Ding, M. Wang and Y. Chen, *RSC Adv.*, 2023, **13**, 24237–24249.

34 Y. Liu, L. Wang, X. Dai, J. Zhang, J. Li, Y. Ma, Q. Han and Y. Dong, *J. Alloys Compd.*, 2024, **976**, 172985.

35 M. Z. Afzal, P. Zu, C. M. Zhang, J. Guan, C. Song, X. F. Sun and S. G. Wang, *J. Hazard. Mater.*, 2022, **434**, 128879.

36 V. Gadore, S. R. Mishra and M. Ahmaruzzaman, *J. Environ. Manage.*, 2023, **334**, 117496.

37 Y. Xie, R. Xiong, J. Li, W. Li, X. Yang and H. Tong, *J. Environ. Manage.*, 2023, **333**, 117428.

38 C. Zhang, H. Li, X. Yang, X. Tan, C. Wan and X. Liu, *J. Environ. Manage.*, 2022, **324**, 116445.

39 G. Cheng, F. Xu, J. Xiong, F. Tian, J. Ding, F. J. Stadler and R. Chen, *Adv. Powder Technol.*, 2016, **27**, 1949–1962.

40 Z. Mengting, T. A. Kurniawan, R. Avtar, M. H. D. Othman, T. Ouyang, H. Yujia, Z. Xueting, T. Setiadi and I. Iswanto, *J. Hazard. Mater.*, 2021, **405**, 123999.

41 C. Nzediegwu, M. Arshad, A. Ulah, M. A. Naeth and S. X. Chang, *Bioresour. Technol.*, 2021, **320**, 124282.

42 J. Fito, K. K. Kefeni and T. T. I. Nkambule, *Sci. Total Environ.*, 2022, **829**, 154648.

43 S. Sutar, S. Otari and J. Jadhav, *Chemosphere*, 2022, **287**, 132200.

44 S.-H. Kong, S.-K. Loh, R. T. Bachmann, S. A. Rahim and J. Salimon, *Renewable Sustainable Energy Rev.*, 2014, **39**, 729–739.

45 B. Yang, J. Dai, Y. Zhao, J. Wu, C. Ji and Y. Zhang, *Biochar*, 2022, **4**, 51.

46 J. Liu, H. Jia, H. Mei, T. Wang, S. Chen and J. Li, *Process Saf. Environ. Prot.*, 2022, **167**, 77–88.

47 S. Ahmad, X. Zhu, X. Wei and S. Zhang, *J. Environ. Manage.*, 2021, **283**, 111981.

48 P. Lisowski, J. C. Colmenares, O. Mašek, D. Łomot, O. Chernyayeva and D. Lisovytskiy, *J. Anal. Appl. Pyrolysis*, 2018, **131**, 35–41.

49 C. Liu, D. Hao, J. Ye, S. Ye, F. Zhou, H. Xie, G. Qin, J. Xu, J. Liu, S. Li and C. Sun, *Adv. Energy Mater.*, 2023, **13**, 2204126.

50 S. Praveen, J. Jegan, T. Bhagavathi Pushpa, R. Gokulan and L. Bulgariu, *Biochar*, 2022, **4**, 10.

51 X. Zhang, Y. Wu, A. S. Giwa, J. Xiong, S. Huang and L. Niu, *Chemosphere*, 2022, **297**, 134152.

52 C. Zhang, W. Xiong, Y. Li, L. Lin, X. Zhou and X. Xiong, *J. Hazard. Mater.*, 2023, **442**, 130013.

53 J. Luo, Y. Wu, M. Jiang, A. Zhang, X. Chen, Y. Zeng, Y. Wang, Y. Zhao and G. Wang, *Chemosphere*, 2023, **311**, 137041.

54 T. Wang, S. Liu, W. Mao, Y. Bai, K. Chiang, K. Shah and J. Paz-Ferreiro, *J. Hazard. Mater.*, 2020, **389**, 121827.

55 L. Kong, Y. Gao, Q. Zhou, X. Zhao and Z. Sun, *J. Hazard. Mater.*, 2018, **343**, 276–284.

56 Z. Zhao, T. Nie and W. Zhou, *Environ. Pollut.*, 2019, **254**, 113015.

57 J. Shi, J. Wang, L. Liang, Z. Xu, Y. Chen, S. Chen, M. Xu, X. Wang and S. Wang, *J. Hazard. Mater.*, 2021, **401**, 123382.

58 J. Du, L. Zhang, T. Liu, R. Xiao, R. Li, D. Guo, L. Qiu, X. Yang and Z. Zhang, *Bioresour. Technol.*, 2019, **274**, 73–82.

59 F. U. Haider, X. Wang, U. Zulfiqar, M. Farooq, S. Hussain, T. Mehmood, M. Naveed, Y. Li, C. Liqun, Q. Saeed, I. Ahmad and A. Mustafa, *Ecotoxicol. Environ. Saf.*, 2022, **248**, 114322.

60 A. El-Naggar, A. H. El-Naggar, S. M. Shaheen, B. Sarkar, S. X. Chang, D. C. W. Tsang, J. Rinklebe and Y. S. Ok, *J. Environ. Manage.*, 2019, **241**, 458–467.

61 H. Shi, M. Wang, B. Wang, Q. Huang and S. Gao, *J. Hazard. Mater.*, 2020, **392**, 122277.

62 S. Ahmad, X. Zhu, Q. Wang, X. Wei and S. Zhang, *J. Anal. Appl. Pyrolysis*, 2021, **160**, 105330.

63 Z.-X. Xu, X.-Q. Deng, S. Zhang, Y.-F. Shen, Y.-Q. Shan, Z.-M. Zhang, R. Luque, P.-G. Duan and X. Hu, *Green Chem.*, 2020, **22**, 3885–3895.

64 W. Cai, J. Wei, Z. Li, Y. Liu, J. Zhou and B. Han, *Colloids Surf., A*, 2019, **563**, 102–111.

65 W. Liu, X. Li, X. Chu, S. Zuo, B. Gao, C. Yao, Z. Li and Y. Chen, *Chemosphere*, 2022, **294**, 133763.

66 J. S. Cha, S. H. Park, S.-C. Jung, C. Ryu, J.-K. Jeon, M.-C. Shin and Y.-K. Park, *J. Ind. Eng. Chem.*, 2016, **40**, 1–15.

67 K. Talukdar, B. M. Jun, Y. Yoon, Y. Kim, A. Fayyaz and C. M. Park, *J. Hazard. Mater.*, 2020, **398**, 123025.

68 F. Chen, M. Zhang, L. Ma, J. Ren, P. Ma, B. Li, N. Wu, Z. Song and L. Huang, *Sci. Total Environ.*, 2020, **730**, 138930.

69 S. Li, S. Harris, A. Anandhi and G. Chen, *J. Cleaner Prod.*, 2019, **215**, 890–902.

70 C. Xia, Y. Liang, X. Li, H. A. Garalleh, M. Garaleh, J. M. Hill and A. Pugazhendhi, *Environ. Res.*, 2023, **218**, 114947.

71 Y. Mei, J. Xu, Y. Zhang, B. Li, S. Fan and H. Xu, *Bioresour. Technol.*, 2021, **325**, 124732.

72 H. Lyu, Q. Zhang and B. Shen, *Chemosphere*, 2020, **240**, 124842.

73 X. Xie, S. Li, H. Zhang, Z. Wang and H. Huang, *Sci. Total Environ.*, 2019, **659**, 529–539.

74 J. Wang and S. Wang, *J. Cleaner Prod.*, 2019, **227**, 1002–1022.

75 H. Zhang, Z. Wang, R. Li, J. Guo, Y. Li, J. Zhu and X. Xie, *Chemosphere*, 2017, **185**, 351–360.

76 D. J. Faheem, S. H. Kim, M. A. Hassan, S. Irshad and J. Bao, *Environ. Sci. Pollut. Res. Int.*, 2020, **27**, 37286–37312.

77 Q. Du, S. Zhang, J. Song, Y. Zhao and F. Yang, *J. Hazard. Mater.*, 2020, **389**, 122115.

78 Y. Lu, Y. Cai, S. Zhang, L. Zhuang, B. Hu, S. Wang, J. Chen and X. Wang, *Biochar*, 2022, **4**, 45.

79 A. Kumar, G. Sharma, M. Naushad, A. H. Al-Muhtaseb, A. Kumar, I. Hira, T. Ahamad, A. A. Ghfar and F. J. Stadler, *J. Environ. Manage.*, 2019, **231**, 1164–1175.

80 Y. Ma, T. Zhang, P. Zhu, Y. Cai, Y. Jin, K. Gao and J. Li, *Sci. Total Environ.*, 2022, **821**, 153453.

81 Y. Wu, H. Cheng, D. Pan, L. Zhang, W. Li, Y. Song, Y. Bian, X. Jiang and J. Han, *J. Environ. Manage.*, 2021, **293**, 112912.

82 D. Guo, D. Feng, Y. Zhang, Z. Zhang, J. Wu, Y. Zhao and S. Sun, *Fuel Process. Technol.*, 2022, **229**, 107200.

83 T. Zheng, S. Ouyang and Q. Zhou, *Biochar*, 2023, **5**, 5.

84 X. Cai, J. Li, Y. Liu, Z. Yan, X. Tan, S. Liu, G. Zeng, Y. Gu, X. Hu and L. Jiang, *J. Chem. Technol. Biotechnol.*, 2017, **93**, 783–791.

85 Q. Huang, S. Song, Z. Chen, B. Hu, J. Chen and X. Wang, *Biochar*, 2019, **1**, 45–73.

86 F. Yu, F. Tian, H. Zou, Z. Ye, C. Peng, J. Huang, Y. Zheng, Y. Zhang, Y. Yang, X. Wei and B. Gao, *J. Hazard. Mater.*, 2021, **415**, 125511.

87 A. Bayles, S. Tian, J. Zhou, L. Yuan, Y. Yuan, C. R. Jacobson, C. Farr, M. Zhang, D. F. Swearer, D. Solti, M. Lou, H. O. Everitt, P. Nordlander and N. J. Halas, *ACS Nano*, 2022, **16**, 5839–5850.

88 J. Schneider, M. Matsuoka, M. Takeuchi, J. Zhang, Y. Horiuchi, M. Anpo and D. W. Bahnemann, *Chem. Rev.*, 2014, **114**, 9919–9986.

89 C. X. Yang, Q. Zhu, W. P. Dong, Y. Q. Fan and W. L. Wang, *Langmuir*, 2021, **37**, 9253–9263.

90 L. Lu, R. Shan, Y. Shi, S. Wang and H. Yuan, *Chemosphere*, 2019, **222**, 391–398.

91 V. Makrigianni, A. Giannakas, C. Daikopoulos, Y. Deligiannakis and I. Konstantinou, *Appl. Catal., B*, 2015, **174–175**, 244–252.

92 T. Xia, Z. Ma, M. Ai, K. Qian, S. Zhu, M. Rong, P. Zhang, Y. Ye and W. Qin, *Chemosphere*, 2021, **267**, 128927.

93 T. Fazal, A. Razzaq, F. Javed, A. Hafeez, N. Rashid, U. S. Amjad, M. S. Ur Rehman, A. Faisal and F. Rehman, *J. Hazard. Mater.*, 2020, **390**, 121623.

94 T. T. Vu Nu, N. H. Thi Tran, P. L. Truong, B. T. Phan, M. T. Nguyen Dinh, V. P. Dinh, T. S. Phan, S. Go, M. Chang, K. T. Loan Trinh and V. Van Tran, *Environ. Res.*, 2022, **206**, 112631.

95 Z. Wu, Y. Xue, Z. Gao, Y. Li, L. Zhang, X. Yang, X. Liu and Z. Chen, *Environ. Sci. Pollut. Res. Int.*, 2021, **28**, 6491–6503.

96 E. O. Oseghe and A. E. Ofomaja, *J. Environ. Manage.*, 2018, **223**, 860–867.

97 S. Silvestri, M. G. Gonçalves, P. A. da Silva Veiga, T. T. d. S. Matos, P. Peralta-Zamora and A. S. Mangrich, *J. Environ. Chem. Eng.*, 2019, **7**, 102879.

98 Y. Tan, W. Zhao, L. Sun, R. Zhang, J. Hou, S. Fu, W. Xu and R. Zhang, *J. Cleaner Prod.*, 2022, **369**, 133280.

99 Z. Xiong, H. Chen, L. Lu, R. Shan, Y. Zhang, H. Yuan and Y. Chen, *ACS Omega*, 2023, **8**, 791–803.

100 Y. Jiang and A. Liu, *Environ. Sci. Pollut. Res. Int.*, 2023, **30**, 31923–31934.

101 Y. Zhou, H. Zhang, L. Cai, J. Guo, Y. Wang, L. Ji and W. Song, *Materials*, 2018, **11**, 1709.

102 M. Penas-Garzon, A. Gomez-Aviles, J. Bedia, J. J. Rodriguez and C. Belver, *Materials*, 2019, **12**, 378.

103 C. Wu, J. Zhang, B. Fang, Y. Cui, Z. Xing, Z. Li and W. Zhou, *J. Cleaner Prod.*, 2021, **329**, 129723.

104 J. R. Kim and E. Kan, *J. Environ. Manage.*, 2016, **180**, 94–101.

105 R. Shan, L. Lu, J. Gu, Y. Zhang, H. Yuan, Y. Chen and B. Luo, *Mater. Sci. Semicond. Process.*, 2020, **114**, 105088.

106 M. M. Mian, G. Liu, B. Yousaf, B. Fu, R. Ahmed, Q. Abbas, M. A. M. Munir and L. Ruijia, *J. Environ. Sci.*, 2019, **78**, 29–41.

107 J. S. Lazarotto, V. Lima Brombilla, S. Silvestri and E. L. Foletto, *Appl. Organomet. Chem.*, 2020, **34**, e6001.

108 C. Bie, H. Yu, B. Cheng, W. Ho, J. Fan and J. Yu, *Adv. Mater.*, 2021, **33**, e2003521.

109 C. Wan, Y. Jiao and J. Li, *Colloid Polym. Sci.*, 2016, **294**, 1281–1287.

110 S. Wang, L. Ji, B. Wu, Q. Gong, Y. Zhu and J. Liang, *Appl. Surf. Sci.*, 2008, **255**, 3263–3266.

111 A. Herath, C. Navarathna, S. Warren, F. Perez, C. U. Pittman Jr and T. E. Mlsna, *J. Colloid Interface Sci.*, 2022, **614**, 603–616.

112 H. Luo, S. Yu, M. Zhong, Y. Han, B. Su and Z. Lei, *J. Alloys Compd.*, 2022, **899**, 163287.

113 Q. Chen, A. Ozkan, B. Chattopadhyay, K. Baert, C. Poleunis, A. Tromont, R. Snyders, A. Delcorte, H. Terryn, M. P. Delplancke-Ogletree, Y. H. Geerts and F. Reniers, *Langmuir*, 2019, **35**, 7161–7168.

114 B. Li, Z. Zhao, Q. Zhou, B. Meng, X. Meng and J. Qiu, *Chemistry*, 2014, **20**, 14763–14770.

115 J. M. Sánchez-Silva, A. Aguilar-Aguilar, G. J. Labrada-Delgado, E. G. Villabona-Leal, H. J. Ojeda-Galván, J. L. Sánchez-García, H. Collins-Martínez, M. V. López-Ramón and R. Ocampo-Pérez, *Environ. Res.*, 2023, **231**, 116280.

116 A. D. Gupta, H. Singh, S. Varjani, M. K. Awasthi, B. S. Giri and A. Pandey, *Sci. Total Environ.*, 2022, **849**, 157831.

117 Y. Dong, W. Du, X. Gao and M. Guo, *J. Cleaner Prod.*, 2022, **365**, 132827.

118 Z. Sun, N. Talreja, H. Tao, J. Texter, M. Muhler, J. Strunk and J. Chen, *Angew Chem. Int. Ed. Engl.*, 2018, **57**, 7610–7627.

119 J. Chung, J. W. Chung and S. Y. Kwak, *Phys. Chem. Chem. Phys.*, 2015, **17**, 17279–17287.

120 P. Lisowski, J. C. Colmenares, O. Mašek, W. Lisowski, D. Lisovytskiy, A. Kamińska and D. Łomot, *ACS Sustainable Chem. Eng.*, 2017, **5**, 6274–6287.

121 Z. Mou, Y. Wu, J. Sun, P. Yang, Y. Du and C. Lu, *ACS Appl. Mater. Interfaces*, 2014, **6**, 13798–13806.

122 S. Zhai, M. Li, D. Wang, L. Zhang, Y. Yang and S. Fu, *J. Cleaner Prod.*, 2019, **220**, 460–474.

123 D. Kanakaraju and A. Chandrasekaran, *Sci. Total Environ.*, 2023, **868**, 161525.

124 C. H. Hsu, W. H. Huang, C. J. Lin, C. H. Huang, Y. C. Chen, K. Kumar, Y. G. Lin, C. L. Dong, M. K. Wu, B. J. Hwang, W. N. Su, S. Y. Chen and C. L. Chen, *Small*, 2023, **19**, e2203881.

125 J. Song, M. Shi, L. Xia, J. Dai, L. Luo, H. Wang, L. Shu and J. Fengzhi, *Chemosphere*, 2023, **333**, 138930.

126 D. V. Thuan, T. T. H. Chu, H. D. T. Thanh, M. V. Le, H. L. Ngo, C. L. Le and H. P. Thi, *Environ. Res.*, 2023, **236**, 116789.

127 M. An, Z. Yang, B. Zhang, B. Xue, G. Xu, W. Chen and S. Wang, *J. Environ. Chem. Eng.*, 2023, **11**, 110367.

128 P. Akhter, F. Ali, A. Ali and M. Hussain, *Diamond Relat. Mater.*, 2024, **141**, 110702.

129 D. Heltina, D. I. Mastura, A. Amri, M. P. Sembiring and Komalasari, *Mater. Today: Proc.*, 2023, **87**, 293–298.

130 S. Samangsri, T. Areerob and S. Chiarakorn, *Res. Chem. Intermed.*, 2022, **49**, 1649–1664.

131 S. Zhang, M. Cai, J. Wu, Z. Wang, X. Lu, K. Li, J.-M. Lee and Y. Min, *Catal. Commun.*, 2023, **174**, 106594.

132 M. Zhang, J. Wang, X. Yuan, Y. Zhang, L. Wang, Y. Xie, Y. Xing and C. Hou, *Appl. Surf. Sci.*, 2023, **637**, 157881.

133 Y. Xie, A. Liu, E. R. Bandala and A. Goonetilleke, *J. Water Process Eng.*, 2022, **48**, 102913.

134 J. Li, N. Liang, X. Jin, D. Zhou, H. Li, M. Wu and B. Pan, *Chemosphere*, 2017, **171**, 66–73.

135 S. Luo, S. Li, S. Zhang, Z. Cheng, T. T. Nguyen and M. Guo, *Sci. Total Environ.*, 2022, **806**, 150662.

136 J. Yu, J. Low, W. Xiao, P. Zhou and M. Jaroniec, *J. Am. Chem. Soc.*, 2014, **136**, 8839–8842.

137 X. Yang, Z. Chen, W. Zhao, C. Liu, X. Qian, M. Zhang, G. Wei, E. Khan, Y. Hau Ng and Y. Sik Ok, *Chem. Eng. J.*, 2021, **405**, 126806.

138 J. Qu, J. Wang, X. Mu, J. Hu, B. Zeng, Y. Lu, M. Sui, R. Li and C. Li, *Adv. Mater.*, 2022, **34**, e2203320.

139 X. Li, S. Anwer, Q. Guan, D. H. Anjum, G. Palmisano and L. Zheng, *Adv. Sci.*, 2022, **9**, e2200346.

140 A. Kumar, P. Choudhary, A. Kumar, P. H. C. Camargo and V. Krishnan, *Small*, 2022, **18**, e2101638.

141 R. Song, H. Chi, Q. Ma, D. Li, X. Wang, W. Gao, H. Wang, X. Wang, Z. Li and C. Li, *J. Am. Chem. Soc.*, 2021, **143**, 13664–13674.

142 P. Zhang, Z. Tian, Y. Kang, B. He, Z. Zhao, C. T. Hung, L. Duan, W. Chen, Y. Tang, J. Yu, L. Mai, Y. F. Li, W. Li and D. Zhao, *J. Am. Chem. Soc.*, 2022, **144**, 20964–20974.

143 G. Wang, W. Feng, X. Zeng, Z. Wang, C. Feng, D. T. McCarthy, A. Deletic and X. Zhang, *Water Res.*, 2016, **94**, 363–370.

144 H. Wang, M. Qu, S. Wang, X. Liu and L. Li, *Adv. Sustainable Syst.*, 2019, **3**, 1800169.